Applied Physics A (2025) 131:897
https://doi.org/10.1007/s00339-025-08896-y

Applied Physics A
Materials Science & Processing

S.I. : NOVEL AND ADVANCED MATERIALS FOR ENERGY AND BIOMEDICAL APPLICATIONS (INEEBA-2024)

Eco-friendly synthesis of Azo-Schiff base metal complexes: evaluation of electrochemical behavior and biological activities

A. Venkatesh[1] · E. Shinyjoy[2] · P. Maheswaran[1] · M. Jeyakanthan[3]

Received: 18 March 2025 / Accepted: 18 August 2025
© The Author(s), under exclusive licence to Springer-Verlag GmbH Germany, part of Springer Nature 2025

Abstract

Azo-Schiff base metal complexes have attracted significant attention due to their diverse applications in industrial and biological fields. In this study, a novel azo-Schiff base ligand was synthesized through the condensation of an azo compound with 2-amino-6-methylpyridine. The ligand was complexed with Co(II), Ni(II), Cu(II), and Zn(II) metal ions in a 1:1 stoichiometry ratio. The resulting metal complexes were characterized using Fourier-transform infrared (FTIR) spectroscopy, proton nuclear magnetic resonance (^{1}H-NMR) spectroscopy, High resolution transmission electron microscope (HRTEM), and molar conductance analysis. The molar conductance values (1–4 $\Omega^{-1}cm^2mol^{-1}$) confirmed the non-electrolytic nature of the complexes, while magnetic moment measurements supported square planar geometry, particularly for Cu(II) ($\mu\_eff = 1.81$ B.M.). Their biological activity was evaluated through in vitro antibacterial testing against Staphylococcus aureus, with the Cu(II) complex exhibiting the highest zone of inhibition (19 mm at 40 µg/mL), indicating strong antibacterial potential. These findings suggest that azo-Schiff base metal complexes could serve as potential candidates for pharmaceutical, industrial, and catalytic applications.

Keywords Azo-Schiff base · Antibacterial activity · Chloroaniline · Salicylaldehyde

1 Introduction

Azo compounds or dyes are characterized by the presence of an azo (-N=N-) moiety, which is conjugated with mono- or polycyclic aromatic or heteroaromatic systems. These compounds exhibit unique physical and chemical properties due to the nitrogen donor atoms in their backbone [1, 2]. They have been widely studied for applications in various fields, including dyeing fibers, photoelectronics, printing systems, optical storage technology, textile dyes, biological interactions, and analytical chemistry [3, 4]. The structural versatility and broad range of applications make azo compounds valuable in many industries. Additionally, azo compounds are extensively explored for their roles in organic synthesis, advanced technology, and biological systems [5].

Azo-Schiff base metal complexes are particularly significant due to their applications in the plastic, leather, and textile industries [6–9]. Moreover, azo dyes play an essential role in industrial processes [10]. These dyes can be categorized into two types based on their coordination properties: those in which the azo group forms a chelate ring with metal ions and those without such coordination [11, 12].

Azo-Schiff base complexes form an important class of ligands that can coordinate with various metal ions to form stable complexes [13–15]. Transition metal complexes derived from these ligands exhibit applications in metal analysis, telecommunications, optical computing, data storage, and information processing. Furthermore, these complexes have shown remarkable biological activities, including antiviral, antitumor, bactericidal, fungicidal, and nonlinear optical properties, making them highly valuable in medicinal and technological fields [15–19].

Additionally, these metal complexes exhibit significant catalytic activity in various organic transformations, such

✉ A. Venkatesh
chemvenk8phd@gmail.com

[1] Department of Chemistry, PGP College of Arts and Science, Namakkal, Tamil Nadu, India

[2] Department of Chemistry, Vinayaka Mission's Kirupananda Variyar Arts and Science College, Vinayaka Mission's Research Foundation (DU), Salem, Tamil Nadu, India

[3] Department of Science (Physics), Sona College of Technology, Salem, Tamil Nadu, India

Published online: 22 October 2025

as oxidation, reduction, and polymerization reactions. They have been explored for their ability to mimic enzymatic functions, providing potential applications in biochemical and pharmaceutical research. Azo-Schiff base metal complexes have also been studied for their electrochemical properties, which contribute to their role in advanced sensor technology and electronic devices. Their tunable electronic properties make them suitable candidates for use in liquid crystals, semiconductors, and smart materials.

Recent advancements in nanotechnology have further expanded the scope of azo-Schiff base metal complexes. Researchers have investigated their potential for forming nanostructured materials, which can be used for targeted drug delivery, photodynamic therapy, and imaging applications. These studies indicate that azo-Schiff base metal complexes are not only crucial in fundamental research but also hold promise for future technological innovations.

In addition to the versatile chemical properties of azo-Schiff base metal complexes, the present study also emphasizes an eco-friendly synthetic approach. The methodology adopted is aligned with green chemistry principles by utilizing ethanol as a benign solvent, operating under mild thermal conditions (ice bath cooling or water bath heating), and avoiding the use of toxic acids, bases, or metal catalysts. The work-up procedure involves minimal solvent use and avoids hazardous waste generation, making the process safe, cost-effective, and environmentally sustainable.

Compared to previously reported studies where focus was given either to spectroscopic characterization or biological evaluation independently, the present work offers a more comprehensive approach. In this study, we report the synthesis of a novel tridentate azo-Schiff base ligand that uniquely coordinates through azomethine nitrogen, phenolic oxygen, and pyridine nitrogen. The work is distinctive in integrating multiple advanced characterization techniques—UV-Vis, FTIR, NMR, XRD, TGA, and cyclic voltammetry—alongside antibacterial studies. Such a combined exploration of electrochemical behavior and biological activity of metal complexes is relatively scarce in existing literature and forms the novelty of this study. This multifaceted evaluation enhances the understanding of structure–property–function relationships and supports the potential application of these complexes in pharmaceuticals and sensor technologies. Furthermore, the eco-friendly synthetic route, along with the dual focus on electrochemical and antimicrobial functionality, makes this study novel in both its methodology and application scope.

2 Synthesis and characterization

2.1 Synthesis of azo-compounds

Chloroaniline (1.38 g) or its derivative was dissolved in HCl (20 mL) and H_2O (5 mL) and heated to 70 °C. The solution was then cooled in an ice bath and diazotized by adding sodium nitrite (0.69 g) dissolved in 3.5 mL of H_2O, maintaining the temperature between 0 and 5 °C. The resulting diazonium salt solution was then added dropwise to a solution of salicylaldehyde (1.05 mL) in H_2O (15 mL) containing sodium hydroxide (0.4 g) and sodium carbonate (7.3 g), over 30 min while maintaining the temperature at 0 °C. The mixture was stirred vigorously throughout the addition. The resulting precipitate was collected by filtration, washed with water, and dried overnight under vacuum at 80 °C. This synthesis approach reflects green chemistry principles by using water and ethanol as solvents, avoiding hazardous reagents, and operating under energy-efficient conditions. The reaction pathway is illustrated in Scheme 1 (Fig. 1).

2.2 Synthesis of 4-((E)-(4-chlorophenyl) diazenyl)−2-((E)-((6-methylpyridin-2 yl)imino) methyl)phen ligand (L)

Equimolar quantities of (E)−5-(2-(4-chlorophenyl) diazenyl)−2-hydroxybenzaldehyde (0.130 g) and 2-amino-6-methylpyridine (0.180 g) were dissolved in 10 mL of warm ethanol and heated in a water bath for 3 h. The reaction mixture was then allowed to stand at room temperature for approximately 24 h, leading to the formation of an orange precipitate. The product was collected by filtration and its purity was confirmed using thin-layer chromatography (TLC). The resulting ligand (L) was then filtered, dried, and stored. The reaction pathway is illustrated in Scheme 2 (Fig. 2).

2.3 Synthesis of schiff base metal (II) complexes

The metal complexes were prepared by reacting the azo-Schiff base ligand (L) with metal salts in appropriate molar

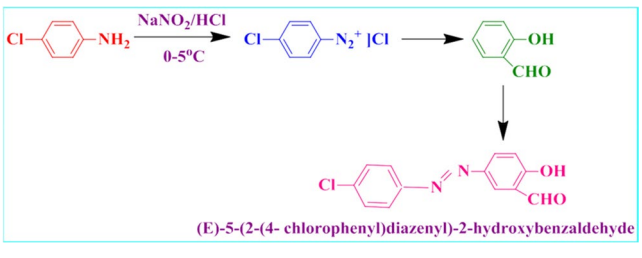

Fig. 1 Synthesis Scheme of azo-compounds

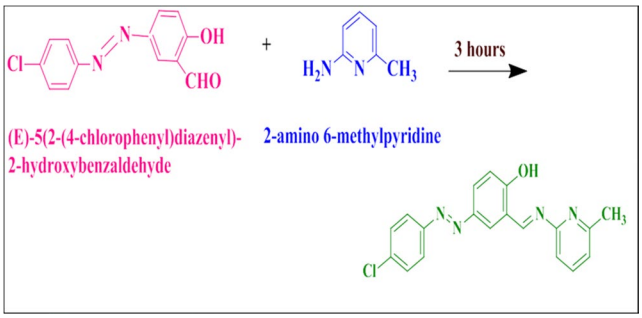

Fig. 2 Synthesis of Schiff base complexes

ratios using the following procedure. A hot ethanolic solution of the metal salt was gradually added to an ethanolic solution of the azo-Schiff base ligand (L) with continuous stirring [19]. The resulting mixture was refluxed for 3 h in a water bath and then allowed to cool to room temperature. The obtained solid product was collected by filtration, washed, and dried. The reaction pathway is illustrated in Fig. 3.

2.4 Characterization

Perkin Elmer elemental analyzer was utilized to obtain the combined compounds (C, H and N). The molar conductance of metal complexes is a crucial aspect of their properties was measured in DMF (10^{-3}) solution was calculated at 27 ± −3 °C. The study utilized KBr discs, a Shimadzu 8300 FTIR spectrophotometer, a THERMO SPECTRONIC 6 HEXIOS for electronic spectra, and an ELICO SL174 for fluorescence spectra. Magnetic susceptibility of the complexes were carried out by the Gouy method using $Hg[Co(SCN)_4]$ as calibrate. NMR spectra were recorded on Brucker AMX400 MHz spectrometer using tetramethylsilane (TMS) as reference.

The antibacterial activity was evaluated against the Gram-positive strain Staphylococcus aureus (ATCC 25923) using the disc diffusion method. MacConkey agar (40 g) was dissolved in distilled water, sterilized by autoclaving at 120 °C for 15 min, and poured into sterile Petri plates. The combined metal complexes (5 mg) were dissolved in acetone

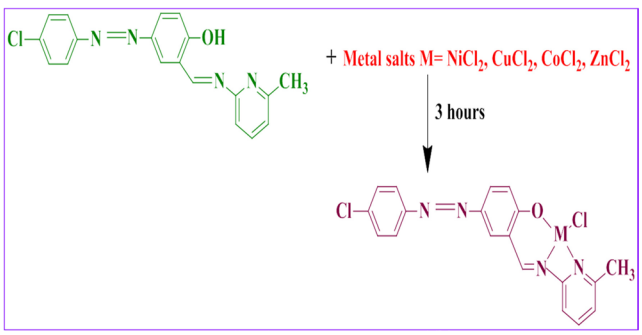

Fig. 3 Synthesis of Mononuclear Schiff base metal complexes

and impregnated on sterile paper discs (6 mm diameter), which were then placed on the inoculated plates using sterilized forceps. A blank disc with only acetone served as the control. The plates were incubated at 37 °C for 48 h. Each test was performed in triplicate ($n=3$) to ensure reproducibility. The antibacterial activity was assessed by measuring the zone of inhibition (in mm) around each disc. The results were expressed as mean ± standard deviation, and statistical analysis was performed using one-way ANOVA to determine significance ($p<0.05$) [20].

3 Results and discussion

3.1 Fourier transmission infrared spectroscopy

The FTIR spectrum was recorded to study the binding of Schiff base ligands to the metal complexes, as shown in Fig. 4. A comparative analysis of the infrared spectra of the free ligand and its metal complexes provides insights into the chelation sites of the ligand molecules. The Schiff base ligand exhibits an intense band in the range of 1621–1563 cm^{-1}, attributed to ν(C=N) stretching, and a broad band at 3450 cm^{-1}, corresponding to the phenolic –OH group [21, 22]. In the metal complexes, a low-frequency shift (10–30 cm^{-1}) is observed around 1610 cm^{-1}, indicating a decrease in the electron density of the azomethine group due to coordination with the metal ion [23]. A characteristic band associated with the ν(N=N) azo bridge vibration appears in the 1456–1499 cm^{-1} range [24].

The band around 3445 cm^{-1}, assigned to the phenolic –OH group in the ligand, disappears in the complexes, confirming coordination through the phenolic oxygen atom via deprotonation [25]. Additionally, bands at 601 cm^{-1} and 458 cm^{-1}, corresponding to in-plane and out-of-plane ring bending, shift to a higher frequency in the complexes, indicating coordination through the pyridine nitrogen.

The coordination of the ligand through azomethine nitrogen (ν(C=N)) and phenolic oxygen (ν(C–O)) is further confirmed by the appearance of new bands in the 416–499 cm^{-1} and 456–516 cm^{-1} regions, attributed to M–N and M–O bonds, respectively [26, 27]. The emergence of a new band in the 310–330 cm^{-1} range in the metal complexes is assigned to ν(M–Cl) stretching vibrations, confirming the coordination of one chlorine atom to the metal ion (Table 1) [28].

3.2 HRTEM and SAED analysis

The morphological and crystallographic nature of the synthesized $C_{19}H_{14}Cl_2N_4OCo$ complex was investigated using High-Resolution Transmission Electron Microscopy (HRTEM) and Selected Area Electron Diffraction (SAED)

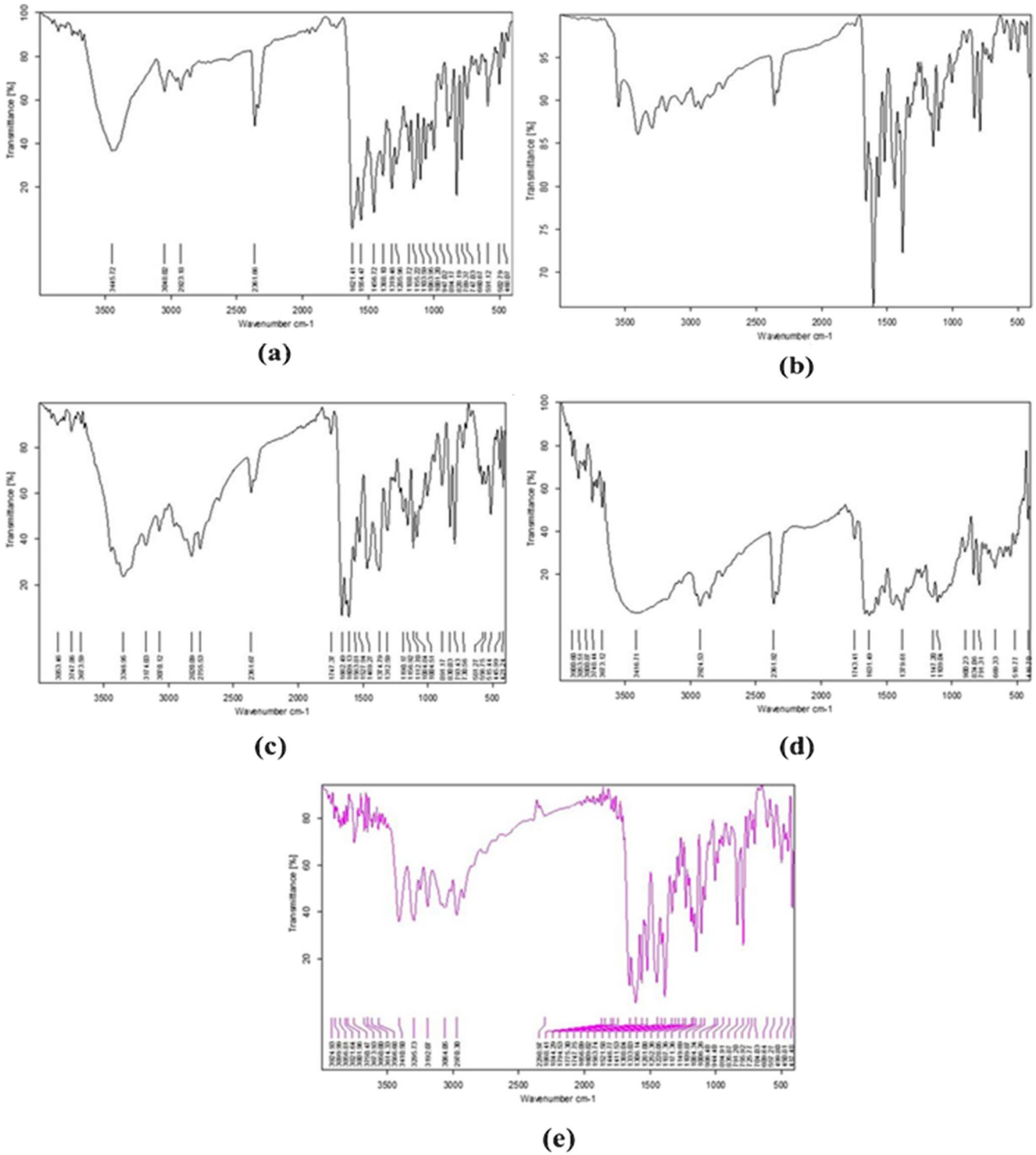

Fig. 4 FTIR spectra of metal complexes (**a**) $C_{19}H_{15}ClN_4O$, (L) (**b**) $C_{19}H_{14}Cl_2N_4OCo$ (Co(II)) (**c**) $C_{19}H_{14}Cl_2N_4OCu$ (Cu(II)) (**d**) $C_{19}H_{14}Cl_2N_4ONi$ (Ni(II)) (**e**) $C_{19}H_{14}Cl_2N_4OZn$ (Zn(II))

analysis. The HRTEM micrograph shown in Fig. 5(a) clearly reveals that the particles are predominantly nanosized with an average diameter ranging from approximately 20 to 90 nm. The particles exhibit well-defined, faceted morphology, suggesting a high degree of crystallinity. The boundaries are sharp, and certain regions display visible lattice fringes, indicating the presence of long-range atomic order and confirming the nanocrystalline nature of the material.

Furthermore, the SAED pattern shown in Fig. 5(b) displays distinct and sharp concentric rings formed by bright diffraction

Table 1 IR absorption frequencies of Azo schiff base ligand and its metal complexes

Complexes	ν (C=*N*) cm-1	ν (O-H) cm-1	ν (M-*N*) cm-1	ν (M-O) cm-1	ν(Ar-Cl) cm-1	ν (C=C) cm-1	bending vibration cm^{-1}	
							NH	CH
L	1621	3445	-	-	789	1456	601	458
Co2+	1563	-	485	511	750	1405	607	478
Cu2+	1606	-	445	515	730	1469	611	486
Ni2+	1610	-	416	516	791	1499	605	475
Zn2+	1609	-	489	523	725	1446	609	480

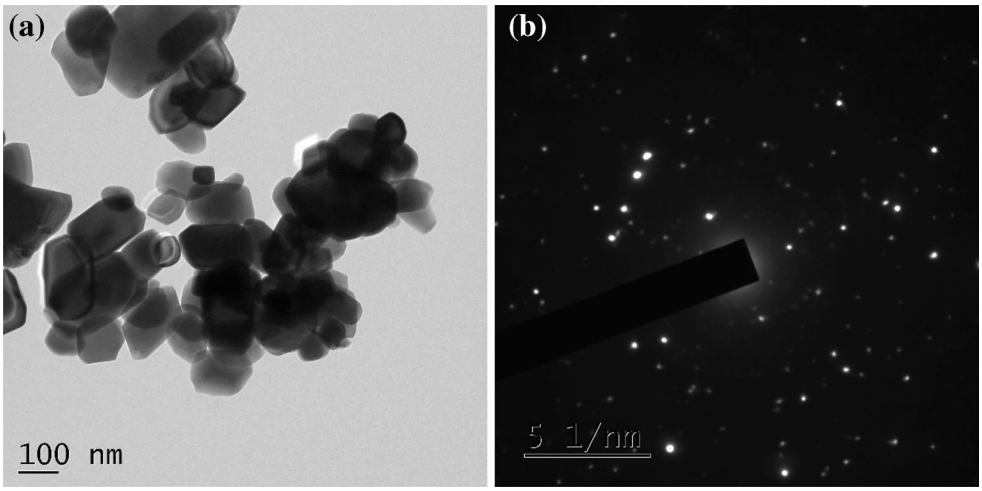

Fig. 5 (**a**) HRTEM image and 5 (**b**) SAED pattern of $C_{19}H_{14}Cl_2N_4OCo$ complex

Table 2 Elemental analysis of Azo schiff base ligand and its metal complexes

Compounds	Molecular formula	Colour	Yield	M.*P* (˚C)	Calcd. (found) %					
					C	H	Cl	*N*	O	M
L	$C_{19}H_{15}ClN_4O$	Orange	68	90±2	65.08 (65.05)	4.28 (4.31)	10.08 (10.1)	15.94 (15.97)	4.53 (4.56)	-
Co2+	$C_{19}H_{14}Cl_2N_4OCo$	Deep blue	70	>300	51.4 (51.01)	3.21 (3.28)	15.99 (15.91)	12.64 (12.67)	3.64 (3.61)	13.31 (13.35)
Cu2+	$C_{19}H_{14}Cl_2N_4OCu$	Dark blue	68	>300	50.88 (50.85)	3.15 (3.14)	15.81 (15.83)	12.51 (12.48)	3.59 (3.56)	14.18 (14.16)
Ni2+	$C_{19}H_{14}Cl_2N_4ONi$	Brown	68	>300	51.44 (51.41)	3.2 (3.18)	15.75 (15.73)	12.65 (12.62)	3.65 (3.61)	13.26 (13.22)
Zn^{2+}	$C_{19}H_{14}Cl_2N_4OZn$	Light brown	72	>280	50.67 (50.65)	3.17 (3.14)	15.77 (15.75)	12.45 (12.42)	3.58 (3.52)	14.54 (14.52)

spots. This pattern confirms the polycrystalline nature of the synthesized complex. The spotty appearance of the rings indicates that the observed area contains multiple well-aligned crystalline domains rather than a fully random polycrystalline matrix. The absence of an amorphous halo and the presence of sharp, indexed diffraction rings provide strong evidence for the formation of a crystalline coordination complex.

The observed diffraction features correspond to the regular arrangement of atoms within the Co(II)-centered coordination lattice, possibly influenced by π-conjugated organic ligands. The crystalline nature as confirmed by both HRTEM and SAED is expected to play a significant role in determining the optical, electrochemical, and biological properties of the complex.

3.3 Elemental analysis

Elemental analysis was carried out to confirm the composition of the synthesized Schiff base ligand (L) and its corresponding metal (II) complexes. The experimental values were found to be in close agreement with the theoretical values, validating the proposed molecular formulae and 1:1

Table 3 Molar conductance of the Azo schiff base ligand and its metal complexes

S.No	Compounds	Solvent	Molar conductance Λ_m ($ohm^{-1}cm^2mol^{-1}$)	Type of electrolyte
1	Co2+	DMF	2.11	Non-electrolyte
2	Cu2+	DMF	3.21	Non-electrolyte
3	Ni2+	DMF	1.18	Non-electrolyte
4	Zn2+	DMF	2.7	Non-electrolyte

metal-to-ligand stoichiometry. The observed minor deviations in elemental percentages may be attributed to experimental conditions and instrumental precision. The presence chemical with quantity is given in Table 2.

Furthermore, the formation of metal complexes is confirmed by the decrease in carbon, hydrogen, and nitrogen content upon complexation, which is consistent with metal coordination. The presence of metal ions was further substantiated through atomic absorption spectroscopy (AAS), while mass spectrometry confirmed the molecular weight of the ligand and its complexes.

3.4 Molar conductance

The molar conductance of the synthesized Schiff base metal (II) complexes was measured in dimethylformamide (DMF) at 27 ± 1 °C to determine their electrolytic behavior. The obtained conductance values ranged between 1 and 4 $\Omega^{-1}cm^2mol^{-1}$, indicating that all the metal complexes exhibit non-electrolytic nature. This suggests that the anions are likely coordinated within the coordination sphere rather than being present as free ions in solution.

The low conductivity values further support the neutral nature of these complexes, implying that no ionic dissociation occurs in solution, which is consistent with their expected covalently bonded structures. The results align with previous studies on similar Schiff base metal complexes, confirming their non-electrolyte character. The molar conductance of the sample given in Table 3.

3.5 Electronic spectra and magnetic moment

UV-Vis spectrum of metal complexes is shown in Fig. 5(a-e). The UV-Vis spectral analysis of the synthesized azo-Schiff base ligands and their metal(II) complexes was carried out in dimethylformamide (DMF) solvent to investigate their electronic transitions and coordination environment. In the free ligand, two characteristic absorption bands were observed at 260 nm and 360 nm, which correspond to $\pi \rightarrow \pi^*$ (aromatic and azo chromophore transitions) and $n \rightarrow \pi^*$ (lone pair transitions on heteroatoms) transitions, respectively [29]. Upon complexation with metal ions, these bands experienced a bathochromic shift (redshift) towards lower energy regions, indicating ligand-to-metal charge transfer (LMCT) interactions. A new absorption band was observed in all metal complexes at 408–424 nm, attributed to ligand-to-metal (L → M) charge transfer, confirming successful coordination and complex formation [30]. Electronic Spectral peak positions of all synthesized ligands and their metal complexes is given Table 4.

The electronic spectrum of the Cu(II) complex exhibited an additional absorption band at 510 nm, which is characteristic of the $^1A_1g \rightarrow {}^1B_1g$ transition. This suggests that the Cu(II) ion adopts a distorted square planar geometry [31]. The magnetic moment of the Cu(II) complex was measured to be 1.81 B.M., further supporting a square planar configuration with a d^9 electronic configuration (one unpaired electron), as shown in Fig. 6.

The electronic spectra of the ligands in DMF revealed a low-intensity band at 260 nm, corresponding to the $\pi \rightarrow \pi^*$ transition, and a moderately intense band at 370 nm, attributed to the $n \rightarrow \pi^*$ excitation. These bands undergo shifts upon complexation, indicating coordination with metal ions. The Ni(II) complex exhibited an absorption band at 586 nm, confirming an octahedral geometry around the Ni(II) ion [32].

For the Co(II) complex, the absorption spectrum displayed a band at 508 nm, assigned to the $^1A_1g \rightarrow {}^1B_1g$ (P) transition, which suggests a distorted square planar geometry around the Co(II) ion. The magnetic moment value of 3.12 B.M. further supports this structural assignment. In contrast, the Zn(II) complex, belonging to the d^{10} system, exhibited diamagnetic behavior, confirming its square planar geometry [33–35].

3.6 ^{1}H-NMR studies

The ^{1}H-NMR spectrum of the synthesized azo-Schiff base ligand (L) was recorded in DMSO-d_6 using tetramethylsilane (TMS) as an internal standard, and is presented in Fig. 7. A distinct singlet observed at δ 9.87 ppm corresponds to the phenolic –OH proton, indicative of intramolecular hydrogen

Table 4 Electronic spectral peak positions of all synthesized ligands and their metal complexes

Complexes	$\pi \rightarrow \pi^*$	$n \rightarrow \pi^*$	L→M	d-d	Transition
L	260	370	-	-	-
Co 2+	252	358	420	508	$^1A_1g \rightarrow {}^1B_1g$
Cu2+	258	360	424	510	$^1A_1g \rightarrow {}^1B_1g$
Ni2+	255	364	412	586	$^2B_1g \rightarrow {}^1A_1g$
Zn2+	256	368	408	-	-

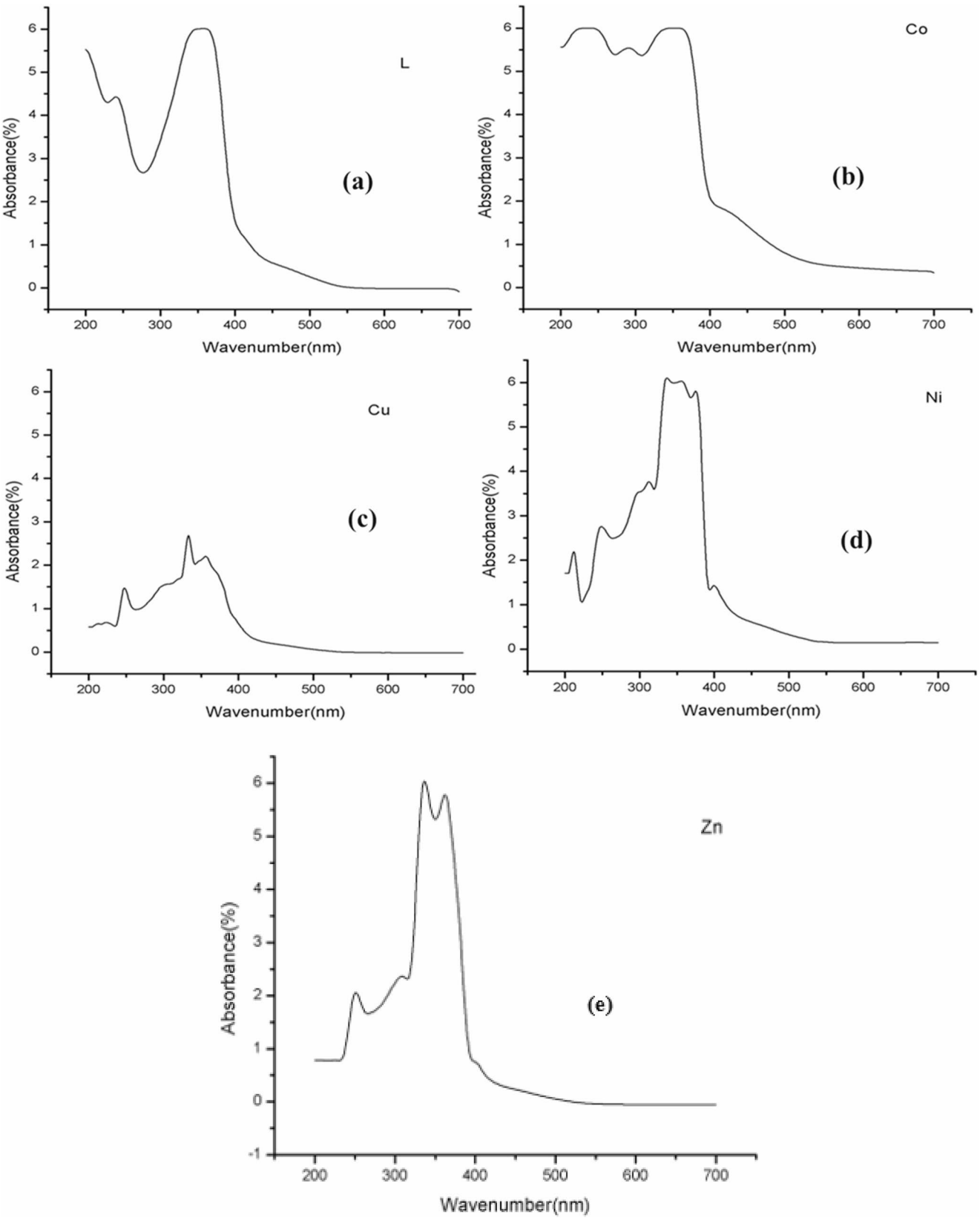

Fig. 6 Electronic spectrum of metal complexes (**a**) $C_{19}H_{15}ClN_4O$, (L) (**b**)$C_{19}H_{14}Cl_2N_4OCo$ (Co(II)) (**c**) $C_{19}H_{14}Cl_2N_4OCu$ (Cu(II)) (**d**) $C_{19}H_{14}Cl_2N_4ONi$ (Ni(II)) (**e**) $C_{19}H_{14}Cl_2N_4OZn$ (Zn(II))

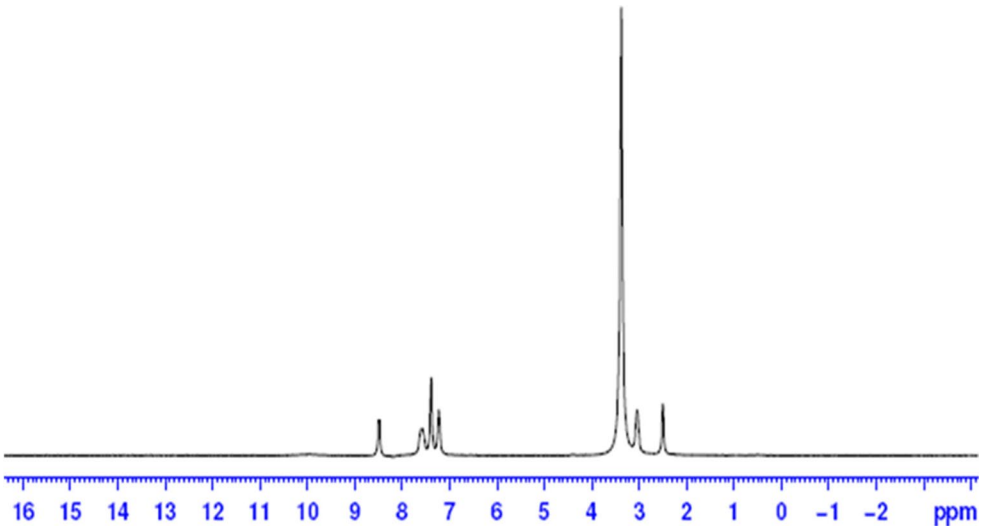

Fig. 7 ^{1}H-NMR spectra of ligand $C_{19}H_{14}ClN_4O$ (L)

bonding. The azomethine proton (–CH=N–) appears as a sharp singlet at δ 8.66 ppm, confirming the successful condensation between the aldehyde and amine moieties. The aromatic region, spanning δ 7.15–8.36 ppm, shows multiple multiplet signals corresponding to the protons of the substituted phenyl and pyridine rings. These signals are consistent with the expected splitting patterns for ortho- and meta-coupled aromatic hydrogens. Additionally, a singlet at δ 2.54 ppm is attributed to the methyl group attached to the pyridine ring. The chemical shift of this signal is slightly downfield due to the deshielding effect exerted by the adjacent nitrogen atom. No additional peaks were observed, confirming the purity of the ligand and the absence of unreacted starting materials. The spectral data strongly support the proposed molecular structure and tridentate coordination capability of the ligand.

3.7 Cyclic voltammetry

Figure 8 Shows the Cyclic voltammetry of metal complexes (a) $C_{19}H_{15}ClN_4O$, (L) (b) $C_{19}H_{14}Cl_2N_4OCo$ (Co(II)) (c) $C_{19}H_{14}Cl_2N_4OCu$ (Cu(II)) (d) $C_{19}H_{14}Cl_2N_4ONi$ (Ni(II)) (e) $C_{19}H_{14}Cl_2N_4OZn$ (Zn(II)). The cyclic voltammetry (CV) analysis was conducted to investigate the redox behavior of the synthesized Schiff base metal(II) complexes in DMF, using tetrabutylammonium perchlorate (TBAP) as the supporting electrolyte. The Cu(II) complex exhibited a one-step redox process, with a cathodic peak corresponding to Cu(II) → Cu(0) reduction at Epc = −0.7 V, and the oxidation peak for Cu(0) → Cu(II) at Epa = 0.5 V. The peak-to-peak separation (ΔEp) increased with the scan rate, exceeding 500 mV, indicating a quasi-reversible redox nature [36, 37]. Additionally, the ratio of anodic to cathodic peak currents (Ipc/Ipa ≈ 1) suggests a stable redox process. The Co(II) complex displayed a quasi-reversible electron transfer with well-defined cathodic reduction and anodic oxidation peaks, exhibiting peak separations of 400 mV and 150 mV, depending on the scan rate. The Ni(II) complex showed a reversible redox process in the −1.3 V to −0.7 V range, attributed to the Ni(II)/Ni(I) redox couple, confirming its electrochemical reversibility. The redox properties were further examined under varying scan rates and potential shifts. The quasi-reversible nature of the Cu(II) and Co(II) complexes is supported by the increased peak-to-peak separation (ΔEp > 500 mV for Cu(II)), indicating slow electron transfer kinetics [38, 39]. The ΔEp values for the Co(II) and Ni(II) complexes ranged between 150 and 400 mV, which fall within the quasi-reversible range. The symmetric shapes of the anodic and cathodic peaks (Ipa ≈ Ipc) and their proportional increase with scan rate support a diffusion-controlled redox mechanism [40, 41]. These findings suggest that the electron transfer between the ligand orbitals and the metal centers is stabilized by the ligand field environment. The electrochemical responsiveness, particularly in the Cu(II) complex, suggests potential applicability in redox-active materials such as sensors, electrocatalysts, or molecular switches. Future studies can explore electrode immobilization and catalytic efficiency to exploit these properties in practical devices [42].

In contrast, the Zn(II) complex did not exhibit distinct redox peaks, as zinc typically maintains a +2 oxidation state, confirming its electrochemical inactivity under the experimental conditions [43]. These electrochemical studies provide strong evidence for the redox behavior of the synthesized metal complexes, further supporting their coordination environments and structural integrity (Table 5; Fig. 8).

The redox-active behavior observed in the Cu(II) and Co(II) complexes suggests their potential use as electrochemical sensors or redox mediators in catalytic systems. Their quasi-reversible nature and stable electron-transfer kinetics make them promising candidates for applications in biosensing, molecular electronics, and electrocatalysis.

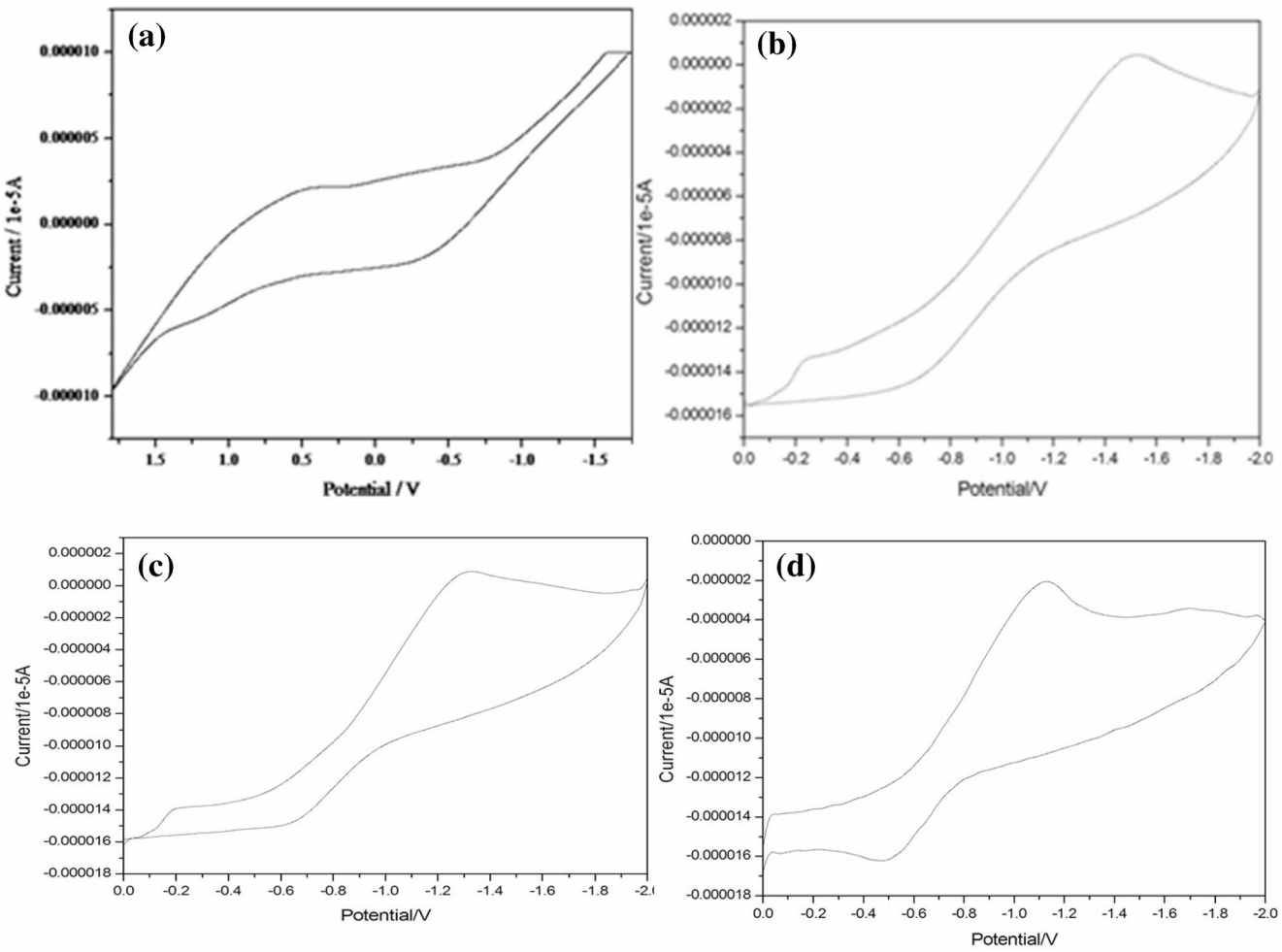

Fig. 8 Cyclic voltammetry of metal complexes (**a**) $C_{19}H_{15}ClN_4O$, (L) (**b**) $C_{19}H_{14}Cl_2N_4OCo$ (Co(II)) (**c**) $C_{19}H_{14}Cl_2N_4OCu$ (Cu(II)) (**d**) $C_{19}H_{14}Cl_2N_4ONi$ (Ni(II)) (**e**) $C_{19}H_{14}Cl_2N_4OZn$ (Zn(II))

Table 5 Electrochemical results of schiff base metal (II) complexes in DMF medium (reduction)

Complexes	E_{pc}(V)	$E_{p.a.}$(V)	$E_{1/2}$(V)	ΔE_P(mV)
Co2+	−0.25	0.5	0.4	1.4
Cu2+	−0.7`	−1.5	0.2	6.7
Ni2+	−0.7	−1.3	0.05	1.18
Zn2+	−0.5	−1.2	0.3	0.95

3.8 Anti-bacterial activity

The antibacterial activity of the synthesized azo-Schiff base metal(II) complexes was evaluated in vitro against Gram-positive bacteria, including *Staphylococcus aureus*. The minimum inhibitory concentration (MIC) values of the metal(II) complexes against different bacterial strains are summarized in Table 6. The results indicate that among all tested metal(II) complexes, the Cu(II) complex exhibited the highest antibacterial activity, showing significant inhibition zones compared to other metal complexes [44].

Table 6 The results of antibacterial studies of Azo schiff base complexes against *Staphylococcus aureus*

Complexes	Concentration			
	10	20	30	40
Zone of inhibition (nm)				
L	2	5	9	12
Cu2+	4	7	14	19
Co2+	3	6	12	18
Ni2+	3	7	12	17
Zn2+	4	7	13	18

Comparative analysis revealed that Ni(II) complexes demonstrated lower antibacterial activity than the parent ligand, suggesting a weaker interaction with bacterial cell membranes. In contrast, the Co(II) and Zn(II) complexes displayed moderate inhibition zones, indicating intermediate antibacterial efficacy. The increased bioactivity of the Cu(II) complex may be attributed to its higher stability and

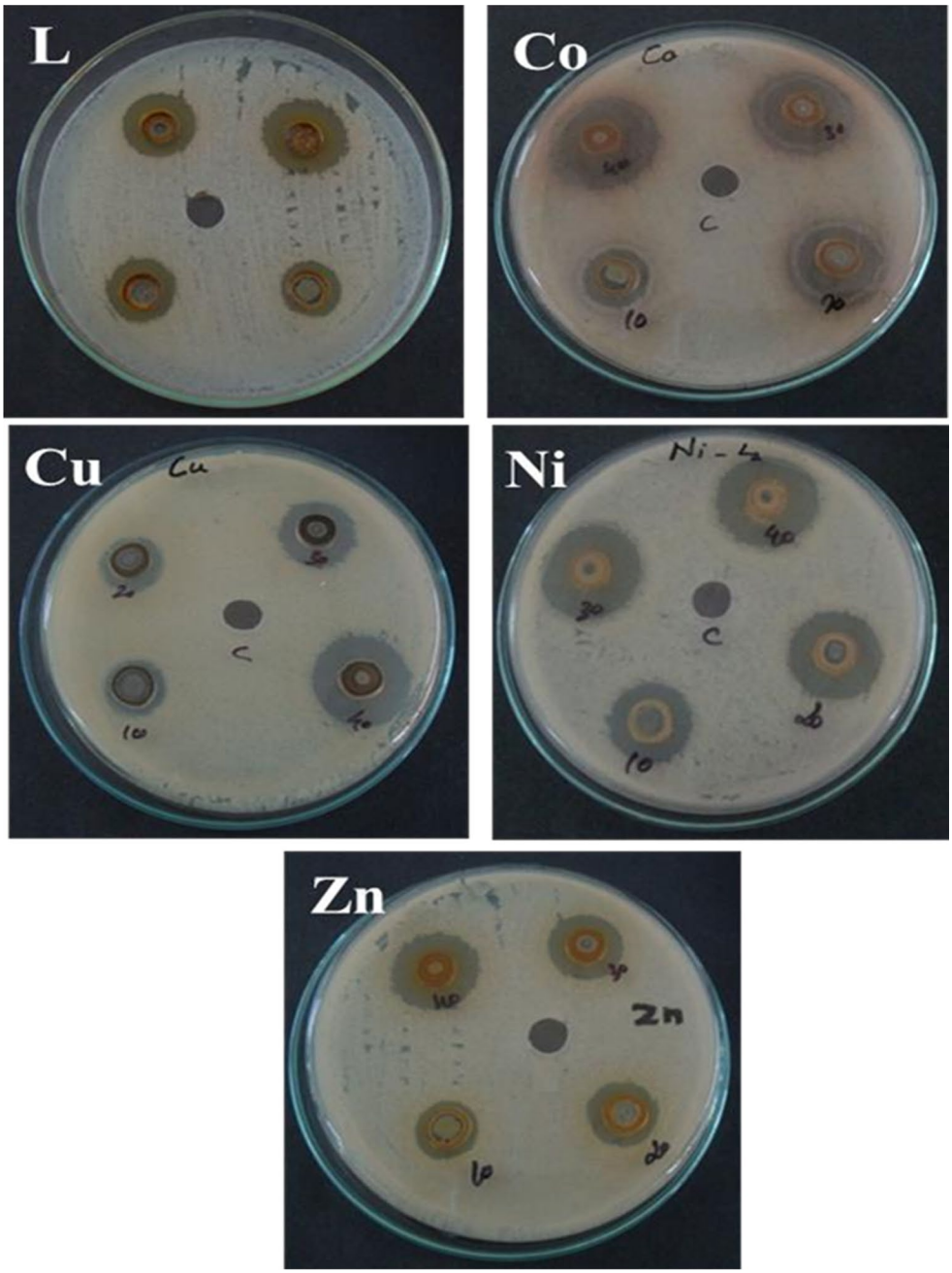

Fig. 9 Antibacterial Activity of Azo Schiff base ligand and its Metal (II) complexes

coordination ability, which enhances its interaction with microbial cell walls, leading to cell damage [45].

These findings confirm that metal coordination significantly enhances the antibacterial potential of Schiff base ligands, particularly in Cu(II) and Zn(II) complexes. The comparative antibacterial effects are graphically represented in Fig. 9, highlighting the variation in inhibition zones across different concentrations. This study suggests that Cu(II)-Schiff base complexes could serve as potential antimicrobial agents, warranting further investigation into their mechanisms of action and broader-spectrum efficacy [46]. The variation in antibacterial activity observed among the metal complexes, as shown in Fig. 9, can be attributed to differences in the coordination environment, ionic radii, and electronic configuration of the metal centers. The Cu(II) complex displayed the highest zone of inhibition, likely due to its smaller ionic radius and greater lipophilicity, which facilitate easier penetration into bacterial membranes. In contrast, the Ni(II) complex exhibited comparatively lower activity, potentially due to reduced membrane permeability and less efficient ligand-metal interaction. The moderate activity of Co(II) and Zn(II) complexes suggests intermediate stability

and interaction with bacterial targets. Coordination of the Schiff base ligand to metal ions increases the overall stability and bioavailability of the complex, thereby enhancing the biological response. These observations are consistent with previously reported structure–activity relationships of similar metal complexes. The superior antibacterial efficacy of the Cu(II) complex observed in this study is consistent with previously reported Schiff base-metal complexes. For example, Schiff base Cu(II) complexes synthesized by Solomon et al. [47] exhibited significant zones of inhibition against S. aureus in the range of 17–20 mm. Similarly, the work of Naik et al. [48] demonstrated enhanced antibacterial activity in Cu(II) complexes due to better cell permeability and chelation effects. The comparable inhibition zones observed in our study (19 mm at 40 µg/mL) validate the effectiveness of our synthesized Cu(II) complex and further highlight its potential as a strong antibacterial agent.

The strong antibacterial performance, particularly of the Cu(II) complex, highlights its potential application as a metal-based antimicrobial agent in pharmaceutical formulations or coating materials to combat bacterial infections.

4 Conclusion

In summary, novel tridentate azo-Schiff base ligands and their Co(II), Ni(II), Cu(II), and Zn(II) complexes were successfully synthesized and structurally confirmed through a combination of spectral (UV-Vis, FTIR, ^{1}H-NMR), electrochemical, and thermal characterization techniques. FTIR and UV-Vis data confirmed metal coordination through azomethine nitrogen and phenolic oxygen, while magnetic moment values supported square planar geometry, particularly for Cu(II). The Cu(II) complex demonstrated the highest antibacterial activity against Staphylococcus aureus with a zone of inhibition measuring 19 mm at 40 µg/mL, confirming its strong antimicrobial potential. Cyclic voltammetry revealed quasi-reversible redox behavior in Cu(II) and Co(II) complexes, suggesting potential applications in redox sensing and molecular electronics. The use of green solvents, mild conditions, and non-toxic reagents reinforces the eco-friendly nature of this synthetic strategy. These findings indicate that azo-Schiff base metal complexes, especially those involving Cu(II), are promising candidates for multifunctional applications in pharmaceuticals, biosensing, and coordination chemistry. Future investigations will focus on exploring cytotoxicity, broader antimicrobial spectra, and nanomaterial hybridization for biomedical applications.

Author contributions **A. Venkatesh**: Validation, Investigation, Visualization and Writing - original draft. **E. Shinyjoy**: Conceptualization, Writing- Review and Editing. **P. Maheswaran**: Validation and Editing. **M. Jeyakanthan**: Review and Editing.

Data availability The authors confirm that the data supporting the findings of this study are available within the article.

Declarations

Conflict of interest The authors declare that they have no known competing financial interests or personal relationships that could have appeared to influence the work reported in this paper.

References

1. B.K. So, M.C. Jang, J.H. Park, K.S. Lee, H.H. Song, S.M. Lee, Opt. Mater. **21**, 685 (2002)
2. Z. Rezvani, B. Divband, A.R. Abbasi, K. Nejati, Polyhedron. **25**, 1915 (2006)
3. M.R. Lutfor, G. Hegde, S. Kumar, C. Tschierske, V.G. Chigrinov, Opt. Mater. **32**, 176 (2009)
4. H. Dinçalp, S. Yavuz, Ö. Haklı, C. Zafer, C. Özsoy, I. Durucasu, S. Içli, J. Photochem. Photobiol A **210**, 8 (2010)
5. C. Motoc, G. Iacobescu, J. Magn. Magn. Mater. **306**, 103 (2006)
6. Z. Zhu, Q. Li, Q. Zeng, Z. Li, Z. Li, J. Qin, C. Ye, Dyes Pigm. **78**, 199 (2008)
7. C. Saravnan, P. Kanan, Polym. Degrad. Stab. **94**, 1001 (2009)
8. P.J. Coelho, L.M. Carvalho, A.M.C. Fonseca, M.M.M. Raposo, Tetrahedron Lett. **47**, 3711 (2006)
9. S.M. Pradeepa, H.S.B. Naik, B.V. Kumar, K.I. Priyadarsini, A. Barik, M.C. Prabhakara, Spectrochim Acta A **141**, 34 (2015)
10. M. Odabasoglu, C. Albayrak, R. Özkanca, F.Z. Akyan, P. Lonecke, J. Mol. Struct. **840**, 71 (2007)
11. E. Ispir, Dyes Pigm. **82**, 13 (2009)
12. S. Issaadi, D. Haffar, T. Douadi, S. Chafaa, D. Seraphin, M.A. Khan, G. Bouet, Synth. React. Inorg. Met.-org. Nan Chem. **35**, 875 (2005)
13. R. Khanum, R.S. Ali, H.R. Rangaswamy, S.R. SanthoshKumar, A.G. Prashantha, A.S. Jagadisha Recent review on Synthesis, spectral Studies, versatile applications of azo dyes and its metal complexes, Results. Chem. **5**, 100890 (2023)
14. A. Bafana, S. Sivanesan, T. Chakrabarti, Environ. Rev. **19**, 350–370 (2011)
15. R.M. Christie, Colour chemistry: Colour: A brief historical perspective (2001). https://doi.org/10.1039/9781847550590-00001
16. F. Eltaboni, N. Bader, R. El-Kailany, N. Elsharif, A. Ahmida, J. Chem. Rev. **4**, 313 (2022)
17. S. Patil, N.A. Choudhary, P.P. Sekar, P. Rathod, Curr. Trends Fashion Technol. Text. Eng. **4**, 555649 (2019)
18. M. Khan, D. Parmar, D. Das, Mini-Rev Med. Chem. **20**, (2020)
19. A. Yousaf, H.A. Shafida, R. Umer, Mini-Rev Med. Chem. **18**, (2018)
20. Z.H. Chohan, H. Pervez, Kausar, Synth. React. Inorg. Met. -org Chem. **32**, 529 (2002)
21. W.J. Geary, Coord. Chem. Rev. **1**, 81 (1971)
22. Z.H. Chohan, S. Kausar, Met. -Based Drugs. **1**, 17 (2000)
23. H. Keypour, S. Salehzadeh, R.V. Parish, Molecules. **7**, 140 (2002)
24. S.M. Annigeri, A.D. Naik, U.B. Gangadharmath, V.K. Revankar, V.B. Mahale, Trans. Met. Chem. **27**, 316 (2002)
25. G.G. Mohamed, M.M. Omar, A.M.M. Hindy, Spectrochim Acta A **62**, 1140 (2005)
26. M.M. Omar, G.G. Mohamed, A.M.M. Hindy, J. Therm. Anal. Calorim. **86**, 315 (2006)
27. G.G. Mohamed, M.M. Omar, A.M.M. Hindy, Turk. J. Chem. **30**, 361 (2006)
28. U. Kamble, S. Patil, P. Badami, J. Incl. Phenom. Macrocycl. Chem. **68**, 347–358 (2010)

29. A.M. Hamil, K.M. Khalifa, A. Al-Houni, M.M. El-Ajailly, Rasayan J. Chem. **2**, 261 (2009)
30. B.T. Thaker, K.R. Surati, J. Coord. Chem. **59**, 1191 (2006)
31. N. Raman, C. Thangaraja, Trans. Met. Chem. **30**, 317 (2005)
32. S. Chandra, L.K. Gupta, D. Jain, Spectrochim Acta A **60**, 2411 (2004)
33. K. Serbest, H. Kayi, M. Er, K. Sancak, I. Degirmencioglu, Heteroat. Chem. **19**, 700 (2008)
34. M. Patel, M. Chhasatia, P. Parmar, Eur. J. Med. Chem. **45**, 439–446 (2010)
35. A. Soroceanu, S. Shova, M. Cazacu, I. Balan, N. Gorinchoy, C. Turta, J. Chem. Cryst. **43**, 310 (2013)
36. J.P. Annaraj, K.M. Ponvel, P. Athappan, Trans. Met. Chem. **29**, 722 (2004)
37. Y. Li, Y. Wu, J. Zhao, P. Yang, J. Inorg. Biochem. **101**, 283 (2007)
38. N.H. Kumar, D. Ravinder, A. Edukondalu, Appl. Phys. A **128**, 978 (2022)
39. B. Baburao, N.H. Kumar, A. Edukondalu, D. Ravinder, Mater. Sci. Eng. B **299**, 116985 (2024)
40. V. Ludhiya, N.H. Kumar, A. Edukondalu, et al. Appl. Phys. A **129**, 614 (2023)
41. Z. Shirin, R.M. Mukherjee, Polyhedron **11**, 2625 (1992)
42. N.H. Kumar, A. Edukondalu, D.J. Ravinder, Aust. Ceram. Soc. **60**, 275–289 (2024)
43. S. Dehghanpour, N. Bouslimani, R. Welter, F. Mojahed, Polyhedron **26,** 154 (2007)
44. E.R. Brown, R.F. Large, in Techniques of Chemistry: Physical Methods of Chemistry,Wiley, New York (1971)
45. K.D. Karlin, P.L. Dahlstrom, J.R. Hyde, J. Zubieta, J. Chem. Soc., Chem. Commun. **1980**, 906
46. P. Shanthakumari, N.H. Kumar, A. Edukondalu, et al. J. Mater. Sci.: Mater.Electron. **34**, 1775 (2023)
47. V.R. Solomon, H. Lee, Eur. J. Med. Chem. **45**, 439–446 (2010)
48. A.D. Naik, H.S. Patel, Spectrochim. Acta A **60**, 2411 (2004)

Publisher's note Springer Nature remains neutral with regard to jurisdictional claims in published maps and institutional affiliations.

Springer Nature or its licensor (e.g. a society or other partner) holds exclusive rights to this article under a publishing agreement with the author(s) or other rightsholder(s); author self-archiving of the accepted manuscript version of this article is solely governed by the terms of such publishing agreement and applicable law.